

Cite this: *RSC Adv.*, 2018, 8, 28209

## Three-dimensional flower-like NiCo<sub>2</sub>O<sub>4</sub>/CNT for efficient catalysis of the oxygen evolution reaction †

Zhaoling Ma,<sup>a</sup> Hao Fu,<sup>a</sup> Cibing Gu,<sup>a</sup> Youguo Huang,<sup>\*a</sup> Sijiang Hu,<sup>b</sup> Qingyu Li<sup>a</sup> and Hongqiang Wang<sup>ID</sup> <sup>\*ab</sup>

The oxygen evolution reaction (OER) is an important reaction especially in water splitting and metal–air batteries. Highly efficient non-noble metal based electrocatalysts are urgently required to be developed and to replace the commercial Ru/Ir based oxide. Herein, we report the three-dimensional hierarchical NiCo<sub>2</sub>O<sub>4</sub>/CNT-150 composite with high activity for the OER that was synthesized *via* a hydrothermal reaction and subsequent annealing. Compared with CNTs, commercial RuO<sub>2</sub> catalysts, NiCo<sub>2</sub>O<sub>4</sub>/CNT, NiCo<sub>2</sub>O<sub>4</sub>/CNT-250, and NiCo<sub>2</sub>O<sub>4</sub>/CNT-150 exhibit enhanced electrocatalytic performance with a lower onset overpotential of 300 mV and the corresponding Tafel slope of 129 mV per decade. The flower-like NiCo<sub>2</sub>O<sub>4</sub>/CNT-150 shows an excellent catalysis performance with higher current density than the commercial RuO<sub>2</sub> catalyst. Moreover, the NiCo<sub>2</sub>O<sub>4</sub>/CNT-150 demonstrates the excellent long-term durability in 0.1 mol L<sup>−1</sup> KOH for the OER. The significant catalytic performances are ascribed to the excellent conductivity of CNTs and the high specific surface area of the three dimensional flower-like NiCo<sub>2</sub>O<sub>4</sub>.

Received 2nd July 2018

Accepted 30th July 2018

DOI: 10.1039/c8ra05639k

rsc.li/rsc-advances

## Introduction

With the increasing consumption of fossil fuels and the continuing increase in environmental pollution, the development of alternative energy conversion or storage devices, such as metal–air batteries and regenerative fuel cells *etc.*, with high power and large energy densities is of particular significance.<sup>1,2</sup> The oxygen reduction reaction (ORR) and oxygen evolution reaction (OER) accompany the charge and discharge process in the cathode of metal–air batteries. In particular, production of hydrogen and oxygen from alkaline water splitting is a potential route to produce clean energy resources. However, the OERs are involved in a wide range of electrochemical processes and their kinetics are sluggish even after being facilitated by noble-metal catalysts.<sup>3</sup>

It is noted that the OER process is complex, with hydroxyl ions being consumed to produce oxygen and water molecules ( $4\text{OH}^- \leftrightarrow \text{O}_2 + 2\text{H}_2\text{O} + 4\text{e}^-$ ), requiring a large overpotential ( $\eta$ ) under alkaline conditions.<sup>4</sup> Up to now, the efficiency of water splitting is not satisfactory. Hence, numerous research efforts have been paid to develop more efficient and stable electrocatalysts to reduce the required overpotential for OER.

Noble-metal based catalysts such as IrO<sub>2</sub> and RuO<sub>2</sub> have emerged as the most promising catalyst candidates for the OER, but their widespread applications in real industry are limited due to the scarcity and high cost.<sup>5</sup> Therefore, in order to realize overall water splitting, the electrocatalysts composing of inexpensive and more abundant materials such as manganese (Mn),<sup>6</sup> and cobalt (Co)<sup>7</sup> are highly desired. To date, among the various electrocatalysts for OER, cobalt-based electrocatalysts are considered to be one of the best performing materials, and the spinel oxides (Co<sub>3</sub>O<sub>4</sub>) have been reported to have high electrochemical performance with low overpotential and excellent chemical stability.<sup>8</sup> To further improve the electrochemical activity of Co<sub>3</sub>O<sub>4</sub> electrocatalysts, researchers have doped Ni atoms into the spinel structure to form NiCo<sub>2</sub>O<sub>4</sub>, which increased electrical conductivity of the metal oxide (at least 2 orders of magnitude higher than that of Co<sub>3</sub>O<sub>4</sub>) and enhanced the catalytic activity for the OER.<sup>9</sup> In addition, spinel NiCo<sub>2</sub>O<sub>4</sub> is easy to form a mesoporous superstructure, which has been studied extensively to investigate the morphological effect on its electrochemical activity.<sup>10,11</sup> More importantly, because of the different valence states in the spinel structure where Ni occupies the octahedral sites and Co occupies both the octahedral and the tetrahedral sites, both redox couples (Co<sup>3+</sup>/Co<sup>2+</sup> and Ni<sup>3+</sup>/Ni<sup>2+</sup>) ensure a notable electrocatalytic activity.<sup>12</sup> Inspired by these good features, several strategies, including sol-gel,<sup>13</sup> hydrothermal,<sup>14</sup> and potentiostatic deposition,<sup>15</sup> have been applied to synthesize various NiCo<sub>2</sub>O<sub>4</sub> nanostructures, such as nanoparticle, nanosheet, nanotube, and NiCo<sub>2</sub>O<sub>4</sub>-based composite

<sup>a</sup>Guangxi Key Laboratory of Low Carbon Energy Materials, School of Chemistry and Pharmaceutical Sciences, Guangxi Normal University, Guilin, 541004, China. E-mail: whq74@126.com; whq74@mailbox.gxnu.edu.cn; Fax: +86-0773-5858562

<sup>b</sup>Hubei Key Laboratory for Processing and Application of Catalytic Materials, College of Chemical Engineering, Huanggang Normal University, Huanggang, 438000, China

† Electronic supplementary information (ESI) available. See DOI: 10.1039/c8ra05639k

*etc.* However, in most cases,  $\text{NiCo}_2\text{O}_4$  still encounters intrinsically low electrical conductivity.<sup>16,17</sup> The most efficient strategies is to choose carbon material as the conductive support for  $\text{NiCo}_2\text{O}_4$  owing to its excellent conductivity.

Carbon nanotube (CNT), as an important class of nano-carbon materials, possesses remarkable electronic conductivity,<sup>18</sup> chemical stability and high specific surface. This enables them to be the good substrate for preparing hybrid and composite materials. Especially, many multi-walled CNT based composites have been exploited as advanced electrocatalysts.<sup>19,20</sup> For OER application, various transition metal or compounds, such as the inexpensive metal compounds,<sup>21,22</sup> and  $\text{MnCo}_2\text{O}_4$ ,<sup>23</sup>  $\text{Ni}(\text{OH})_2$ ,<sup>24</sup>  $\text{Co}(\text{OH})_2$ ,<sup>25</sup> have been grown on CNTs in attempts to improve the OER performances. This has been confirmed to be a feasible and effective method. The present works on  $\text{NiCo}_2\text{O}_4/\text{CNT}$  composite with 3D hierarchical structure could arouse an attractive potential OER electrocatalyst.

In this work, we construct a three-dimensional hierarchical  $\text{NiCo}_2\text{O}_4/\text{CNT}$  network electrode for OER by a potentiostatic electrodeposition technique followed by a calcination-annealing process in the air. In this typical binder-free electrode, the CNTs vertically grown on Ti foil are used as “rod” to support the 3D flower-like  $\text{NiCo}_2\text{O}_4$  nanosheet, which would not only remarkably improve outstanding conductivity but also notably increase the specific surface area. The excellent performance is credited to the specific micro-structure and the remarkable synergistic effects of the components. In view of the highly increased catalytic function in the OER, the  $\text{NiCo}_2\text{O}_4/\text{CNT}$  composite proves to be a very promising candidate as an electrocatalyst for water splitting.

## Materials and methods

### Growth of CNTs on Ti foil substrate

All reagents were of analytical grade and were directly used without further purification. All the solutions were prepared with deionized water. Ti foil (purity 99.999%,  $\sim 0.1$  mm in thickness, Baoji Titanium products Co. Ltd.) were used as substrate for growth of self-propped CNTs layer. First, Ti foil was cleaned by ultrasonication respectively with absolute ethanol and deionized water. The Ti foil was further decontaminated in the solution containing  $15\text{ g L}^{-1}$  NaOH,  $20\text{ g L}^{-1}$   $\text{Na}_2\text{CO}_3$  and  $5\text{ mmol L}^{-1}$  OP emulsifier at  $60^\circ\text{C}$  for 15 min. Secondly, it is subsequently immersed in a mixed acid solution containing hydrochloric acid (25% v/v) and hydrofluoric acid (5% v/v) for 2 min. Thirdly, Ni catalyst particles were deposited on Ti foil by electroless deposition in the solution containing  $500\text{ mmol L}^{-1}$  glycol,  $20\text{ g L}^{-1}$  nickel chloride and  $15\text{ g L}^{-1}$  ammonium fluoride at  $60^\circ\text{C}$  for 5 min. CNTs were grown on Ti foil by chemical vapor deposition (CVD) process.  $\text{C}_2\text{H}_2$  is used as carbon source under  $\text{H}_2$  atmosphere at the pressure of 20 kPa. The growth time of CNTs was controlled for 40 min.

### Preparation of $\text{NiCo}_2\text{O}_4/\text{CNT}$ electrode

Prior to preparation, the CNT/Ti substrate ( $1.5\text{ cm} \times 2\text{ cm}$ ) was immersed in absolute ethanol for 10 min. The well-treated CNT/

Ti substrate was transferred into the solution containing 1 mmol  $\text{Ni}(\text{NO}_3)_2 \cdot 6\text{H}_2\text{O}$ , 2 mmol  $\text{Co}(\text{NO}_3)_2 \cdot 6\text{H}_2\text{O}$ , 2 mmol  $\text{NH}_4\text{F}$ , and 6 mmol  $\text{CO}(\text{NH}_2)_2$ . The solvent is comprised with 40 mL ethanol and 40 mL  $\text{H}_2\text{O}$ . The solution including CNT/Ti substrate was transferred into 100 mL Teflon-lined stainless autoclave, followed by hydrothermal synthesis at  $100^\circ\text{C}$  for 10 h. The obtained precursor was washed several times by water and dried at  $50^\circ\text{C}$  (labeled as  $\text{NiCo}_2\text{O}_4/\text{CNT}$ ). The other samples were synthesized as similar method except for the different subsequent annealing temperature at  $150^\circ\text{C}$  and  $250^\circ\text{C}$ . The dried precursor was calcined for 2 h with a ramp rate of  $5^\circ\text{C min}^{-1}$ . The resulted samples were denoted as  $\text{NiCo}_2\text{O}_4/\text{CNT-150}$  and  $\text{NiCo}_2\text{O}_4/\text{CNT-250}$ . The CNTs peeled from CNT/Ti substrate was denoted as CNT. The quality of  $\text{NiCo}_2\text{O}_4$  in  $\text{NiCo}_2\text{O}_4/\text{CNT-150}$  and  $\text{NiCo}_2\text{O}_4/\text{CNT-250}$  was respectively  $0.55\text{ mg}$  ( $\sim 0.19\text{ mg cm}^{-2}$ ) and  $0.28\text{ mg}$  ( $\sim 0.10\text{ mg cm}^{-2}$ ).

### Materials characterization

The surface morphology and structure of the samples were analyzed by Field Emission Scanning Electron Microscopy (FE-SEM, FEI Quanta 200 FEG, Holland) and transmission electron microscope (TEM, FEI TECNAI D2 12, Holland). Electron diffraction spectroscopy (EDS) was applied to determine the elements of powders together with SEM in large field of view. X-ray photoelectron spectroscopy (XPS) was carried out on a Physical Electronics 5400 ESCA. The crystalline structure of the samples were analyzed by X-ray diffraction (XRD) on a D/Max-2500V/PC powder diffractometer equipped with  $\text{Cu K}\alpha$  radiation ( $k = 0.15406\text{ nm}$ ) (Rigaku, Tokyo, Japan). The Fourier transform infrared spectra were recorded using a Nicolet 6700 spectrometer (Thermo Scientific, USA). All physical characterization of CNT,  $\text{NiCo}_2\text{O}_4/\text{CNT-150}$  and  $\text{NiCo}_2\text{O}_4/\text{CNT-250}$  were carried out on Ti substrates.

### Electrochemical measurements

All the electrochemical measurements were conducted in a three-electrode cell on a CHI 660e electrochemical workstation (Chenhua, Shanghai). All materials were peeled from Ti substrate and executed electrochemical measurements.  $0.1\text{ mol L}^{-1}$  KOH was used as the electrolyte. A saturated calomel electrode (SCE) and Pt sheet were respectively used as reference electrode and counter electrode.  $\text{NiCo}_2\text{O}_4/\text{CNT}$ ,  $\text{NiCo}_2\text{O}_4/\text{CNT-150}$ ,  $\text{NiCo}_2\text{O}_4/\text{CNT-250}$  and  $\text{NiCo}_2\text{O}_4/\text{CNT-150}$ ,  $\text{NiCo}_2\text{O}_4/\text{CNT-250}$  and commercial  $\text{RuO}_2$  were made into  $2\text{ mg mL}^{-1}$  catalyst inks, which contain  $995\text{ }\mu\text{L}$  water,  $995\text{ }\mu\text{L}$  ethanol as well as  $10\text{ }\mu\text{L}$  of 5 wt% Nafion solution. The  $20\text{ }\mu\text{L}$  catalyst inks were loaded on the glass carbon electrodes with 4 mm diameter as the working electrodes. Linear scan voltammetry (LSV) was conducted from 0 to  $0.8\text{ V}$  with a scan rate of  $5\text{ mV s}^{-1}$  for the polarization curves and Tafel slopes. The stability was analyzed by chronoamperometry which was carried out at  $1.63\text{ V}$  versus RHE. Electrochemical impedance spectroscopy (EIS) was performed in the frequency range of  $0.1\text{ Hz}$  to  $100\text{ kHz}$  at  $0.63\text{ V}$  versus SCE. All electrochemical tests were collected under  $\text{O}_2$  saturation to ensure the  $\text{O}_2/\text{H}_2\text{O}$  equilibrium at  $1.23\text{ V}$ . The reported potentials in this work are versus reversible hydrogen



electrode (RHE), which is based on the Nernst equation ( $E_{\text{RHE}} = E_{\text{SCE}} + 0.059 \text{ pH} + 0.2412$ ). The overpotential ( $\eta$ ) was calculated according to the formula:  $\eta \text{ (V)} = E_{\text{RHE}} - 1.23$ . All the potential values were compensated by eliminating  $iR$  drop from ohmic resistance of the electrolytes.

## Results and discussion

The synthesis process of the 3D flower-like  $\text{NiCo}_2\text{O}_4$  on CNT is shown in Scheme 1. Ti foil was worked as the substrate. CNTs are vertically grown on the Ti foil by CVD process with the Ni-based catalysts, which could possess a high degree of graphitization. Subsequently, the 3D flower-like  $\text{NiCo}_2\text{O}_4$  are prepared *via* hydrothermal reaction and subsequent calcination. In  $\text{NiCo}_2\text{O}_4/\text{CNT}$  composite, vertically grown CNTs offer excellent electrical conductivity for rapid electron transport. Furthermore, 3D flower-like  $\text{NiCo}_2\text{O}_4$  could show the large surface area, which could not only provide more active area for OER but also form the whole conductive networks.

The synthesized CNT,  $\text{NiCo}_2\text{O}_4/\text{CNT}$ ,  $\text{NiCo}_2\text{O}_4/\text{CNT-150}$  and  $\text{NiCo}_2\text{O}_4/\text{CNT-250}$  composites were characterized by FTIR spectroscopy, and the results are shown in Fig. S1.† For CNT, the bands at  $\sim 3300 \text{ cm}^{-1}$ ,  $\sim 2955 \text{ cm}^{-1}$ ,  $\sim 1620 \text{ cm}^{-1}$ ,  $\sim 1260 \text{ cm}^{-1}$  and  $1090 \text{ cm}^{-1}$  represent respectively hydroxyl ( $-\text{OH}$ ), carbon-hydrogen bonds ( $-\text{CH}_3$ ), carbon-carbon bonds ( $-\text{C}=\text{C}-$ ), carboxyl ( $-\text{COOH}$ ) and carbon-oxygen bonds ( $\text{C}-\text{O}$ ),<sup>26–28</sup> whose appearance suggests the slight oxidation existed on the as-grown CNTs and it could provide the sites for the subsequent growth of  $\text{NiCo}_2\text{O}_4$ . The bands at  $\sim 810 \text{ cm}^{-1}$  and  $660 \text{ cm}^{-1}$  are attributed to the carbon-hydrogen bonds ( $\text{C}-\text{H}$ ) of aromatic nucleus in carbon skeleton.<sup>28,29</sup> In the case of the  $\text{NiCo}_2\text{O}_4/\text{CNT}$ ,  $\text{NiCo}_2\text{O}_4/\text{CNT-150}$  and  $\text{NiCo}_2\text{O}_4/\text{CNT-250}$ , all the characteristic peaks are same as the counterpart of CNT except of the shifts towards lower wavenumber, which suggests the successful hybrid connection of CNT and  $\text{NiCo}_2\text{O}_4$ .

XRD measurements were used to identify the chemical composition and phase of the as-prepared electrocatalysts. Fig. 1 shows the XRD patterns obtained from CNT,  $\text{NiCo}_2\text{O}_4/\text{CNT}$ ,  $\text{NiCo}_2\text{O}_4/\text{CNT-150}$  and  $\text{NiCo}_2\text{O}_4/\text{CNT-250}$ . CNT shows a typical diffraction peak at  $\sim 27.3^\circ$  corresponding to the (331) plane of CNT. However, five dominant diffraction peaks at  $\sim 21^\circ$ ,  $\sim 38.4^\circ$ ,  $\sim 40^\circ$ ,  $\sim 53^\circ$ ,  $\sim 70.5^\circ$  and  $77^\circ$  corresponding to the (120), (002), (101), (102), (103) and (201) plane reflections of the Ti foil substrate. Notably, the peaks at  $\sim 18.8^\circ$  and  $\sim 59.1^\circ$  of  $\text{NiCo}_2\text{O}_4/\text{CNT}$  and  $\text{NiCo}_2\text{O}_4/\text{CNT-150}$  are respectively belonged to (111) and (511) planes of the cubic spinel  $\text{NiCo}_2\text{O}_4$  (JCPDS no.

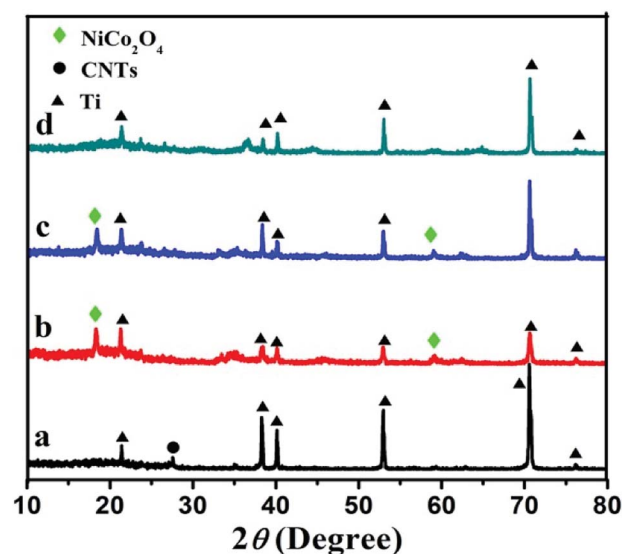
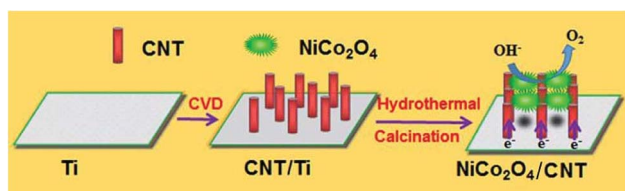


Fig. 1 X-ray powder diffraction patterns obtained for CNT (a),  $\text{NiCo}_2\text{O}_4/\text{CNT}$  (b),  $\text{NiCo}_2\text{O}_4/\text{CNT-150}$  (c),  $\text{NiCo}_2\text{O}_4/\text{CNT-250}$  (d).

20-0781),<sup>30</sup> where nickel atoms located at octahedral sites and cobalt atoms occupied both octahedral and tetrahedral sites.<sup>31</sup> Nevertheless, the two peaks are not observed in  $\text{NiCo}_2\text{O}_4/\text{CNT-250}$ , which means that the higher calcination temperature enabled to deteriorate the crystalline structure.

The morphology of the resulted composites was shown in Fig. 2. Fig. 2a shows the CNTs with the diameter of about 50 nm fabricated directly on Ti substrate surface by CVD. These CNTs are grown vertically and possess the diameter about 30 to 70 nm. Fig. 2b show the  $\text{NiCo}_2\text{O}_4$  before annealing has been grown uniformly on the CNTs. The connection of nanosheets constitute into the flowerlike  $\text{NiCo}_2\text{O}_4$ . Undergoing the annealing at  $150^\circ\text{C}$ , the flowerlike  $\text{NiCo}_2\text{O}_4$  of  $\text{NiCo}_2\text{O}_4/\text{CNT-150}$



Scheme 1 The synthesis processes of 3D flower-like  $\text{NiCo}_2\text{O}_4/\text{CNT}$  on Ti foil.

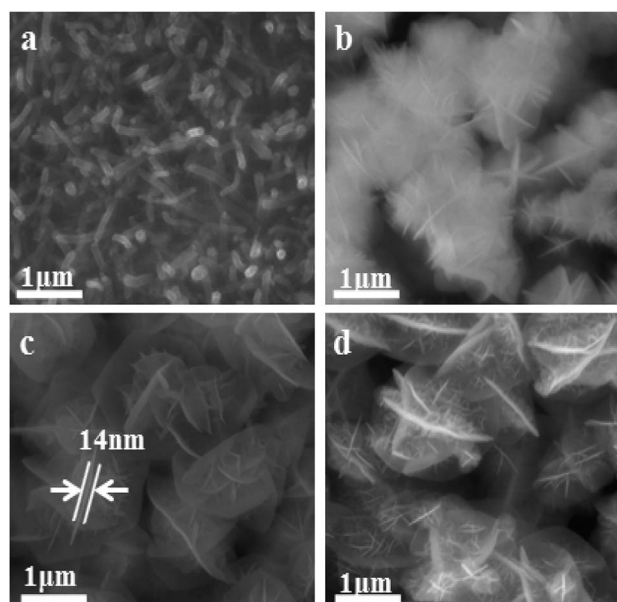


Fig. 2 SEM images of (a) CNT and (b)  $\text{NiCo}_2\text{O}_4/\text{CNT}$ ; (c)  $\text{NiCo}_2\text{O}_4/\text{CNT-150}$  and (d)  $\text{NiCo}_2\text{O}_4/\text{CNT-250}$ .





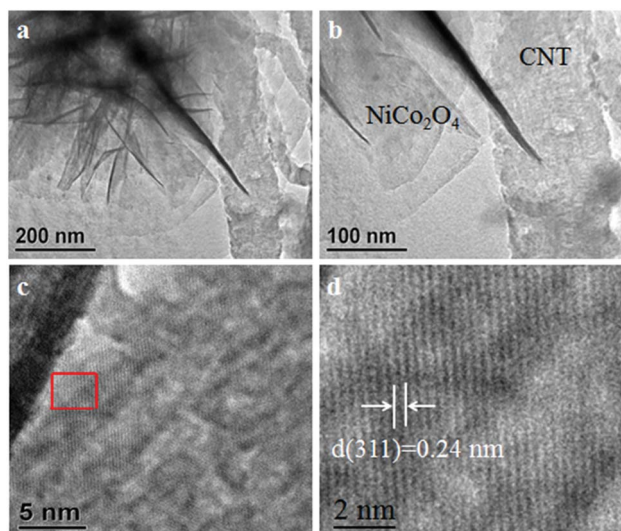


Fig. 3 (a and b) TEM images and (c and d) HRTEM images of  $\text{NiCo}_2\text{O}_4/\text{CNT-150}$ .

150 in Fig. 2c has the diameter of about  $1.5\ \mu\text{m}$  and exhibits clear nanosheets and surface wrinkles. Moreover,  $\text{NiCo}_2\text{O}_4$  flower closely connected with each other, which is benefit to rapid transport electrons. The  $\text{NiCo}_2\text{O}_4$  nanosheets show the thickness of approximately 14 nm. The surface wrinkles can afford more active sites for OER. When the annealing temperature was increased to  $250\ ^\circ\text{C}$ ,  $\text{NiCo}_2\text{O}_4$  nanosheets changed into a number of nanothorns.

In order to determine the corresponding elemental mappings of  $\text{NiCo}_2\text{O}_4/\text{CNT-150}$ , elemental mapping by EDS spectrum was used to analyze elements distribution. The EDS analysis in Fig. S2† further corroborates its uniform deposition. As seen, the elements C, O, Co and Ni of  $\text{NiCo}_2\text{O}_4/\text{CNT-150}$  are evenly distributed in the selected area, indicating the uniform  $\text{NiCo}_2\text{O}_4$  flowers deposition on the surface of CNT.

These CNTs and 3D flower-like  $\text{NiCo}_2\text{O}_4$  were further characterized by transmission electron microscopy (TEM) as shown in Fig. 3. It was observed that flower-like nanosheets of  $\text{NiCo}_2\text{O}_4/\text{CNT-150}$  connect tightly to the CNTs substrate (Fig. 3a and b). This confirms the close contact between the 3D  $\text{NiCo}_2\text{O}_4$

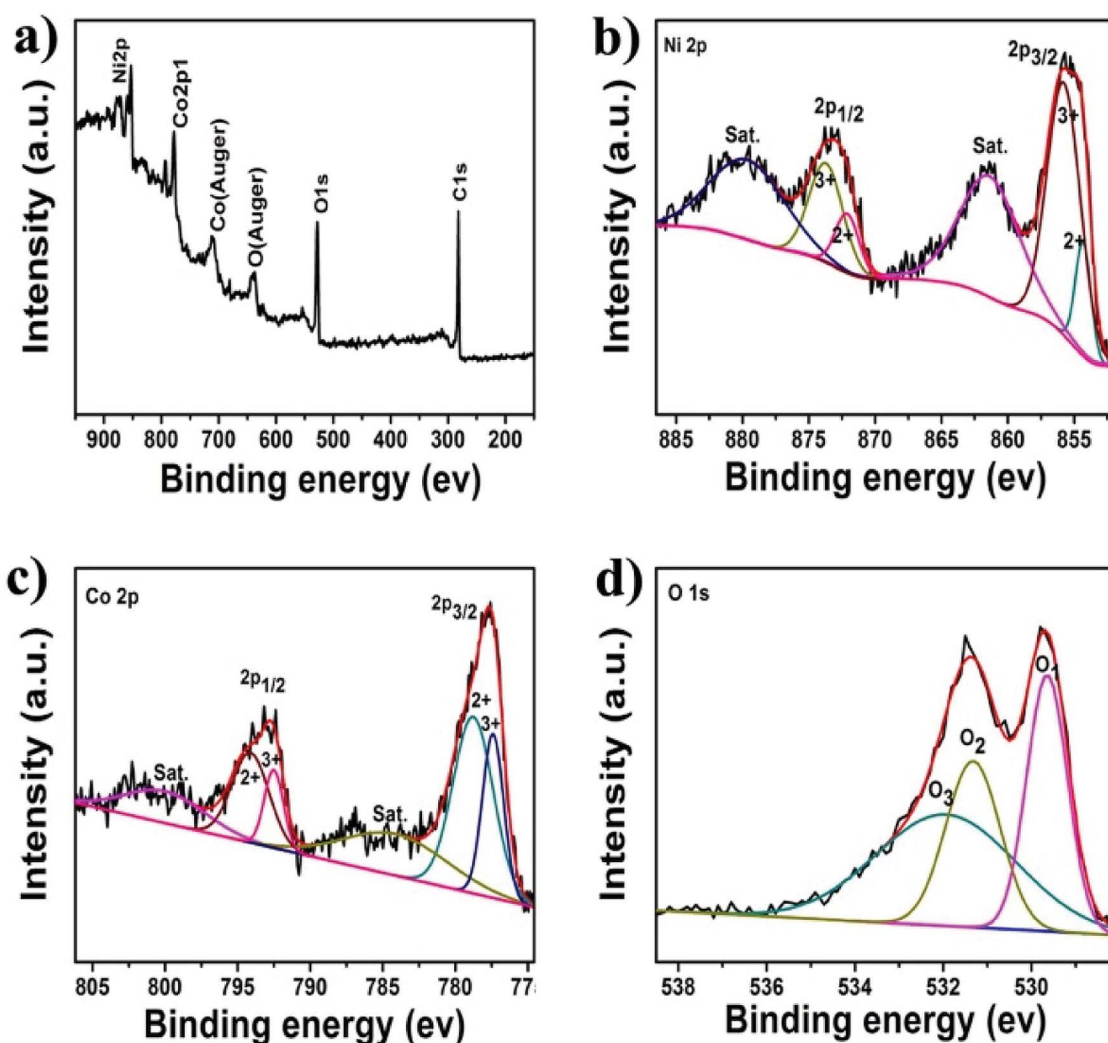


Fig. 4 XPS spectra of (a) survey spectrum, (b) Ni 2p, (c) Co 2p and (d) O 1s for  $\text{NiCo}_2\text{O}_4/\text{CNT-150}$ .



nanosheets and CNTs scaffold. The blurry lattice fringes in Fig. 3c testify the low crystallinity of  $\text{NiCo}_2\text{O}_4/\text{CNT-150}$ . The interplanar distance of 0.24 nm is corresponded to the (311) plane of  $\text{NiCo}_2\text{O}_4$  (Fig. 3d). Clearly, the  $\text{NiCo}_2\text{O}_4$  crystals in  $\text{NiCo}_2\text{O}_4/\text{CNT-150}$  shows discontinuous lattice fringes. That means that abundant of crystal defects exists on the surface of  $\text{NiCo}_2\text{O}_4$ , especially for the (311) plane. It could provide a quantity of crystal defects as the new type of catalytic sites for OER.

To investigate the chemical state of the as-prepared electrocatalysts, XPS technique was used to analysis  $\text{NiCo}_2\text{O}_4/\text{CNT-150}$ . As shown in Fig. 4a, the survey spectrum indicates the presence of Ni, Co, O and C element without other impurity elements. The Ni 2p spectrum in Fig. 4b can be fitted as two shakeup satellites (indicated as "Sat.") and two spin-orbit doublets characteristic of  $\text{Ni}^{2+}$  and  $\text{Ni}^{3+}$  with Gaussian fitting.<sup>32</sup> The peaks at 855.9 eV and 873.4 eV are assigned to  $\text{Ni}^{3+}$ , while the peaks at 854.2 eV and 871.6 eV are belonged to  $\text{Ni}^{2+}$ .<sup>33,34</sup> It is implied that two nickel ions exist in  $\text{NiCo}_2\text{O}_4$ . The satellite peaks located at 861.5 eV and 879.3 eV are two overlapping type peaks.<sup>35</sup> Similarly, the Co 2p spectrum, as shown in Fig. 4c, also can be fitted into two satellites as well as two spin-orbit peaks, characteristics of  $\text{Co}^{2+}$  and  $\text{Co}^{3+}$ .<sup>16</sup> The O 1s spectrum in Fig. 4d, shows

three chemical states of oxygen element, respectively labeled as  $\text{O}_1$ ,  $\text{O}_2$  and  $\text{O}_3$ . The  $\text{O}_1$  peak at 529.5 eV corresponds to metal-oxygen bonds.<sup>36</sup> The  $\text{O}_2$  peak at 531.3 eV is assigned to  $\text{OH}^-$  groups, indicating that carbon nanotubes is partly hydroxylated as a result of surface hydroxides.<sup>37</sup> The  $\text{O}_3$  peak located at 532.2 eV is identified to the physical adsorbed water.<sup>38</sup> Obviously, the XPS data illustrates that the electron couples of  $\text{Ni}^{3+}/\text{Ni}^{2+}$  and  $\text{Co}^{3+}/\text{Co}^{2+}$  are concomitant in the as-prepared  $\text{NiCo}_2\text{O}_4$  sample.

The electrochemical performance of the  $\text{NiCo}_2\text{O}_4/\text{CNT}$  composite was investigated in 0.1 M KOH solution, as shown in Fig. 5. Fig. 5a shows the polarization curves of CNT,  $\text{NiCo}_2\text{O}_4/\text{CNT}$ ,  $\text{NiCo}_2\text{O}_4/\text{CNT-150}$ ,  $\text{NiCo}_2\text{O}_4/\text{CNT-250}$  and commercial  $\text{RuO}_2$  electrodes. Obviously,  $\text{NiCo}_2\text{O}_4/\text{CNT-150}$  electrode exhibits the most superior OER performance than other electrodes. The onset overpotential of  $\text{NiCo}_2\text{O}_4/\text{CNT-150}$  was 300 mV, which is lower than  $\text{NiCo}_2\text{O}_4/\text{CNT}$  (340 mV),  $\text{NiCo}_2\text{O}_4/\text{CNT-250}$  (390 mV). The overpotentials for  $\text{NiCo}_2\text{O}_4/\text{CNT-150}$  at  $10 \text{ mA cm}^{-2}$  and  $100 \text{ mA cm}^{-2}$  was 330 mV and 470 mV smaller than that of  $\text{NiCo}_2\text{O}_4/\text{CNT}$ ,  $\text{NiCo}_2\text{O}_4/\text{CNT-250}$  and commercial  $\text{RuO}_2$ . Comparison with other reported electrocatalyst material was summarized in Table S1.† The overpotential of  $\text{NiCo}_2\text{O}_4/\text{CNT-150}$  is even lower than the water oxidation catalyst Au/

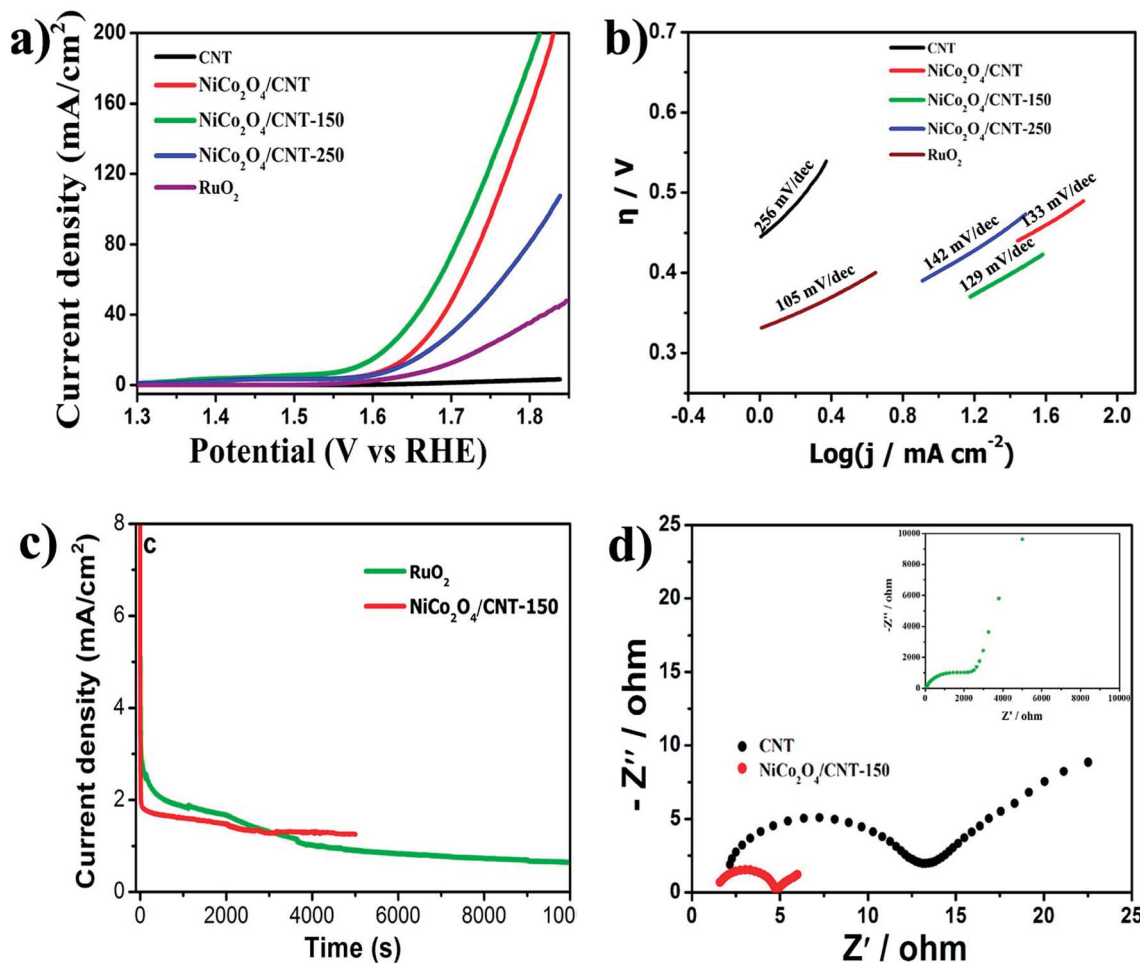


Fig. 5 (a) LSV curves, (b) Tafel plots, (c) stability measurement and (d) EIS spectra of CNT,  $\text{NiCo}_2\text{O}_4/\text{CNT}$ ,  $\text{NiCo}_2\text{O}_4/\text{CNT-150}$ ,  $\text{NiCo}_2\text{O}_4/\text{CNT-250}$  and  $\text{RuO}_2$  electrodes.



NiCo<sub>2</sub>O<sub>4</sub> nanorod array with the overpotential of 360 mV at 10 mV cm<sup>-2</sup>. These results further confirm the lattice defects on 3D flower-like NiCo<sub>2</sub>O<sub>4</sub>/CNT-150 may be more beneficial for affording more catalytic sites, effectively increasing catalytic activity area and further strengthening the OER performance. The Tafel behavior, especially the Tafel slope, is an important OER kinetic parameter. The superior kinetics of NiCo<sub>2</sub>O<sub>4</sub>/CNT-150 was confirmed by the correspondingly lower Tafel slope of 129 mV dec<sup>-1</sup>, compared with that of NiCo<sub>2</sub>O<sub>4</sub>/CNT (133 mV dec<sup>-1</sup>), NiCo<sub>2</sub>O<sub>4</sub>/CNT-250 (142 mV dec<sup>-1</sup>), CNT (256 mV dec<sup>-1</sup>) and commercial RuO<sub>2</sub> (105 mV dec<sup>-1</sup>), as shown in Fig. 5b. The results confirm that NiCo<sub>2</sub>O<sub>4</sub>/CNT-150 possesses efficient kinetics for OER. The high catalytic activity is of very importance for the large scope application in the water splitting.

The stability of OER on the as-synthesized electrocatalysts was investigated at 1.63 V *versus* RHE using chronoamperometry, as presented in Fig. 5c. Due to the production of oxygen, the electrocatalysts was happened to fall off from the electrode and thus the time of the stability measurement is controlled at 5000 s for NiCo<sub>2</sub>O<sub>4</sub>/CNT-150 and 10000 s for the commercial RuO<sub>2</sub>. Obviously, at initial 3000 s in Fig. 5c, the commercial RuO<sub>2</sub> has better stability even if the current densities of the commercial RuO<sub>2</sub> and NiCo<sub>2</sub>O<sub>4</sub>/CNT-150 both gradually decrease. The current density of NiCo<sub>2</sub>O<sub>4</sub>/CNT-150, however, remains hardly change after about 3000 s in contrast to the lasting decrease of the current density of the commercial RuO<sub>2</sub>. It is demonstrated that NiCo<sub>2</sub>O<sub>4</sub>/CNT-150 has better electrocatalytic stability. The electrochemical impedance spectra (EIS) obtained at 1.63 V (*vs.* RHE) was shown in Fig. 5d. In the high frequency region, the solution resistance is region from the interface resistance between the electrolyte and the electrode.<sup>39</sup> NiCo<sub>2</sub>O<sub>4</sub>/CNT-150 shows the lowest solution resistance of only 1.3 Ω. In low frequency region, it is clear that the NiCo<sub>2</sub>O<sub>4</sub>/CNT-150 still shows the lowest charge transfer resistance, indicating the rapid electron transport during OER process in contrast to the CNT and the commercial RuO<sub>2</sub> seen in the inset of Fig. 5b. Therefore, the CVD growth enables NiCo<sub>2</sub>O<sub>4</sub> and CNT to form integral electrical conductor, facilitating the accelerated electrochemical kinetics and contributing to a superior electrochemical performance for OER.

The morphology and structure changes of NiCo<sub>2</sub>O<sub>4</sub>/CNT-150 electrode after all the electrochemical characterization were investigated by SEM and XRD, as shown in Fig. S3 and S4.† Fig. S3† shows the unchanged morphology of the NiCo<sub>2</sub>O<sub>4</sub>/CNT-150. Both the size and flower shape were still remained compared with the sample before electrochemical characterization in Fig. 2c. XRD spectra in Fig. S4† further demonstrated the outstanding stability of NiCo<sub>2</sub>O<sub>4</sub>/CNT-150, where it held nearly the same phase composition and crystal structure. The result further confirmed an excellent stability of NiCo<sub>2</sub>O<sub>4</sub>/CNT-150 in electrochemical process.

## Conclusions

In this work, 3D flower-like NiCo<sub>2</sub>O<sub>4</sub> spheres were successfully prepared on CNTs by CVD growth combined with the

hydrothermal method. The morphology of NiCo<sub>2</sub>O<sub>4</sub> on CNTs was readily controlled *via* adjusting the subsequent calcination temperature. The as-prepared NiCo<sub>2</sub>O<sub>4</sub>/CNT-150 composite shows lower overpotential, larger current density and higher electrochemical stability. The onset overpotential of NiCo<sub>2</sub>O<sub>4</sub>/CNT-150 is 300 mV, which was lower than NiCo<sub>2</sub>O<sub>4</sub>/CNT-250 (390 mV). Furthermore, The overpotential at 10 mA cm<sup>-2</sup> current density for NiCo<sub>2</sub>O<sub>4</sub>/CNT-150 is 330 mV smaller than that of commercial RuO<sub>2</sub>. The superior kinetics of NiCo<sub>2</sub>O<sub>4</sub>/CNT-150 is confirmed by the corresponding lower Tafel slope of 129 mV dec<sup>-1</sup>, compared with that of NiCo<sub>2</sub>O<sub>4</sub>/CNT (133 mV dec<sup>-1</sup>), NiCo<sub>2</sub>O<sub>4</sub>/CNT-250 (142 mV dec<sup>-1</sup>) as well as CNT (256 mV dec<sup>-1</sup>), which are mainly ascribed to the ascendant conductivity of CNT substrate and the 3D flower shape of NiCo<sub>2</sub>O<sub>4</sub>. All these characteristics are greatly beneficial for oxygen evolution reaction. This work offers a strategy to enhance the OER performance of NiCo<sub>2</sub>O<sub>4</sub> on CVD grown carbon by effectively increasing the electrical conductivity of NiCo<sub>2</sub>O<sub>4</sub>.

## Conflicts of interest

This work has not been published previously. It is not under consideration for publication elsewhere, and its publication is approved by all authors and tacitly or explicitly by the responsible authorities where the work was carried out. If accepted, it will not be published elsewhere in the same form, in English or in any other language, without the written consent of the Publisher.

## Acknowledgements

Financial supports from the National Natural Science Foundation of China (U1401246, 51474110, 51474077 and 21473042) are gratefully acknowledged.

## References

- 1 L. Zeng, X. Cui, J. Zhang, W. Huang, L. Chen, C. Wei and J. Shi, *Electrochim. Acta*, 2018, **275**, 218–224.
- 2 M. Zhang, M. Respinis and H. Frei, *Nat. Matter.*, 2014, **6**, 362–367.
- 3 C. Wu, Y. Zhang, D. Dong, H. Xie and J. Li, *Nanoscale*, 2017, **9**, 12432–12440.
- 4 B. S. Yeo and A. T. Bell, *J. Am. Chem. Soc.*, 2011, **133**, 5587–5593.
- 5 Y. Wang, C. Xie, Z. Zhang, D. Liu, R. Chen and S. Wang, *Adv. Funct. Mater.*, 2018, **28**, 1703363.
- 6 Y. Zhao, C. Chang, F. Teng, Y. Zhao, G. Chen, R. Shi, G. I. N. Waterhouse, W. Huang and T. Zhang, *Adv. Energy Mater.*, 2017, **7**, 1700005.
- 7 C. A. Kent, J. J. Concepcion, C. J. Dares, D. A. Torelli, A. J. Rieth, A. S. Miller, P. G. Hoertz and T. J. Meye, *J. Am. Chem. Soc.*, 2013, **135**, 8432–8435.
- 8 X. Deng and H. Tuysuz, *ACS Catal.*, 2014, **4**, 3701–3714.
- 9 B. Lu, D. Cao, P. Wang, G. Wang and Y. Gao, *Int. J. Hydrogen Energy*, 2011, **36**, 72–78.



- 10 H. Wang, Q. Gao and L. Jiang, *Small*, 2011, **7**, 2454–2459.
- 11 C. Yuan, J. Li, L. Hou, L. Yang, L. Shen and X. Zhang, *J. Mater. Chem.*, 2012, **22**, 16084–16090.
- 12 H. Cheng, Y. Z. Su, P. Y. Kuang, G. F. Chen and Z. Q. Liu, *J. Mater. Chem. A*, 2015, **3**, 19314–19321.
- 13 R. Ding, L. Qi and H. Wang, *J. Solid State Electrochem.*, 2012, **16**, 3621–3633.
- 14 X. Y. Liu, Y. Q. Zhang, X. H. Xia, S. J. Shi, Y. Lu, X. L. Wang, C. D. Gu and J. P. Tu, *J. Power Sources*, 2013, **239**, 157–163.
- 15 W. Liu, C. Lu, K. Liang and B. K. Tay, *J. Mater. Chem. A*, 2014, **2**, 5100–5107.
- 16 C. Chang, L. Zhang, C. W. Hsu, *et al.*, *ACS Appl. Mater. Interfaces*, 2017, **357**, 238–246.
- 17 J. Deng, H. Zhang, Y. Zhang, P. Luo, L. Liu and Y. Wang, *J. Power Sources*, 2017, **372**, 46–53.
- 18 T. W. Ebbesen, H. J. Lezec, H. Hiura, J. W. Bennett, H. F. Ghaemi and T. Thio, *Nature*, 1996, **382**, 54–56.
- 19 X. Chen, H. Zhu, Y. C. Chen, Y. Shang, A. Cao, L. Hu and G. W. Rubloff, *ACS Nano*, 2012, **6**, 7948–7955.
- 20 M. Sun, G. Zhang, H. Liu, Y. Liu and J. Li, *Sci. China Mater.*, 2015, **58**, 683–692.
- 21 Y. Cheng, C. Liu, H. M. Cheng and S. P. Jiang, *ACS Appl. Mater. Interfaces*, 2014, **6**, 10089–10098.
- 22 M. Liu and J. Li, *Electrochim. Acta*, 2015, **154**, 177–183.
- 23 X. Ge, Y. Liu, F. W. Hor, T. S. Andy Hor, Y. Zong, P. Xiao, Z. Zhang, S. H. Lim, B. Li, X. Wan and Z. Liu, *ACS Appl. Mater. Interfaces*, 2014, **6**, 12684–12691.
- 24 Z. Tang, C.-h. Tang and H. Gong, *Adv. Funct. Mater.*, 2012, **22**, 1272–1278.
- 25 J. Zhang, X. Wang, J. Ma, S. Liu and X. Yi, *Electrochim. Acta*, 2013, **104**, 110–116.
- 26 Y. Zhuo, J. Liu, Q. Li, B. Qiu and G. Xing, *Integr. Ferroelectr.*, 2016, **171**, 52–58.
- 27 M. U. Khan, V. G. Gomes and I. S. Altarawneh, *Carbon*, 2010, **48**, 2925–2933.
- 28 P. S. Thomas, A. A. Abdullateef, M. A. Al-Harthi, A. A. Basfar, S. Bandyopadhyay, M. A. Atieh and S. K. De, *J. Appl. Polym. Sci.*, 2012, **124**, 2370–2376.
- 29 A. Gromov, S. Dittmer, J. Svensson, O. A. Nerushev, S. A. Perez-García and L. Licea-Jiménez, *J. Mater. Chem.*, 2005, **15**, 3334–3339.
- 30 G. Q. Zhang, H. B. Wu, H. E. Hoster, M. B. Chan-Park and X. W. Lou, *Energy Environ. Sci.*, 2012, **5**, 9453–9456.
- 31 L. Shen, Q. Che, H. Li and X. Zhang, *Adv. Funct. Mater.*, 2014, **24**, 2630–2637.
- 32 J. Liang, Z. Y. Fan, S. Chen, S. J. Ding and G. Yang, *Chem. Mater.*, 2014, **26**, 4354–4360.
- 33 J. F. Marco, J. R. Gancedo, M. Gracia, J. L. Gautier, E. I. Rios, H. M. Palmer, C. Greaves and F. J. Berry, *J. Mater. Chem.*, 2015, **11**, 3087–3093.
- 34 C. Yu, L. Zhang, J. Shi, J. Zhao, J. Gao and D. Yan, *Adv. Funct. Mater.*, 2008, **18**, 1544–1554.
- 35 Q. W. Zhou, J. C. Xing, Y. F. Gao, X. J. Lv, Y. M. He, Z. H. Guo and Y. M. Li, *ACS Appl. Mater. Interfaces*, 2014, **6**, 11394–11402.
- 36 C. Z. Yuan, J. Y. Li, L. R. Hou, L. Yang, L. F. Shen and X. G. Zhang, *J. Mater. Chem.*, 2012, **22**, 16084–16090.
- 37 Y. E. Roginskaya, O. V. Morozova, E. N. Lubnin, Y. E. Ulitina, G. V. Lopukhova and S. Trasatti, *Langmuir*, 1997, **13**, 4621–4627.
- 38 T. Y. Wei, C. H. Chen, H. C. Chien, S. Y. Lu and C. C. Hu, *Adv. Mater.*, 2010, **22**, 347–351.
- 39 Y. T. Meng, W. Q. Song, H. Huang, Z. Ren, S. Y. Chen and L. S. Steven, *J. Am. Chem. Soc.*, 2014, **136**, 11452–11464.

